THE JOURNAL OF PHYSICAL CHEMISTRY Letters

Letter

pubs.acs.org/JPCL

$(CH_3NH_3)_2Pb(SCN)_2I_2$: A More Stable Structural Motif for Hybrid Halide Photovoltaics?

Alex M. Ganose,[†,‡] Christopher N. Savory,[†] and David O. Scanlon*[,†,‡]

[†]University College London, Kathleen Lonsdale Materials Chemistry, Department of Chemistry, 20 Gordon Street, London WC1H 0AJ, United Kingdom

[‡]Diamond Light Source, Ltd., Diamond House, Harwell Science and Innovation Campus, Didcot, Oxfordshire OX11 0DE, United Kingdom

Supporting Information

ABSTRACT: Hybrid halide perovskites have recently emerged as a highly efficient class of light absorbers; however, there are increasing concerns over their long-term stability. Recently, incorporation of SCN^- has been suggested as a novel route to improving stability without negatively impacting performance. Intriguingly, despite crystallizing in a 2D layered structure, $(CH_3NH_3)_2Pb(SCN)_2I_2$ (MAPSI) possesses an ideal band gap of 1.53 eV, close to that of the 3D connected champion hybrid perovskite absorber, $CH_3NH_3PbI_3$ (MAPI). Here, we identify, using hybrid density functional theory, the origin of the smaller than expected band gap of MAPSI through a detailed comparison with the electronic structure of MAPI. Furthermore, assessment of the MAPSI structure reveals that it is thermodynamically stable with respect to phase separation, a likely source of the increased stability reported in experiment.

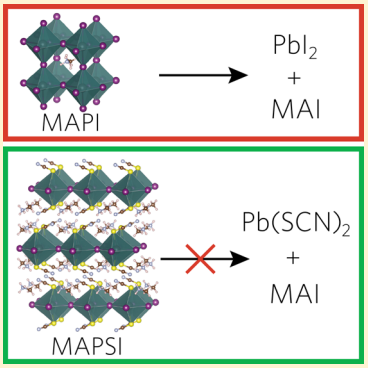

The past three years have witnessed an explosion of interest into hybrid halide perovskite solar cells.[1−3] Power conversion efficiencies (PCEs) have skyrocketed to 20.1%,[4] quickly surpassing other third-generation devices such as dye-sensitized solar cells,[5] organic photovoltaics,[6] and the champion inorganic earth-abundant absorber, $Cu_2ZnSn(S,Se)_4$ (CZTSSe).[7,8] Currently, the highest performing hybrid perovskite is $CH_3NH_3PbI_3$ (MAPI), which can be easily solution processed for widespread application[9−11] and possesses an ideal direct band gap of 1.55 eV,[12] a small exciton binding energy,[13] balanced electron−hole transport with extremely long carrier diffusion lengths,[14,15] defect self-regulation,[16] and excellent charge carrier mobilities.[17−19]

Unfortunately, despite these excellent properties, chemical stability is still a major concern facing hybrid perovskites as they move toward industrial deployment.[20,21] Indeed, while suitable encapsulation should reduce decomposition by hydrolysis,[22−24] the fundamental long-term stability of the MAPI structure is still a topic of dispute.[25] Much effort has been devoted to increasing the stability of MAPI based devices, however, these stable cells generally perform with reduced PCEs of 10−13%.[26−28] Preserving high efficiencies while demonstrating increased chemical and thermodynamic stability is therefore a significant challenge facing the hybrid halide perovskite community.[29]

In the past six months, the substitution of iodine with the pseudohalide ion, SCN^-, has been proposed as a novel method for increasing the stability of MAPI based devices.[30−33] Chen et al. reported that the incorporation of SCN^- (which has a similar ionic radius to I^-) to form $CH_3NH_3PbI_{3-x}(SCN)_x$ resulted in larger crystal sizes and fewer trap states than pure MAPI.[30] The authors reported a PCE of 11% for planar $CH_3NH_3PbI_{3-x}(SCN)_x$/PC61BM bilayer heterojunction solar cells, finding that 5% SCN^- incorporation was the optimum in the range of 1−10%, and that the $CH_3NH_3PbI_{3-x}(SCN)_x$ films displayed greater stability, higher reproducibility, and lower amounts of hysteresis than similarly prepared MAPI films.[34,35] The reason for this extra stability was not elucidated.

Halder et al. subsequently observed that incorporation of SCN^- as a *dopant* opened up the fundamental band gap versus MAPI by 8 meV, and had a remarkable effect on the photoluminescence response, concluding that SCN^- incorporation is a valuable addition to the hybrid halide family.[31]

Jiang et al. recently reported that $CH_3NH_3Pb(SCN)_2I$ films crystallized in the perovskite structure, with a band gap of 1.53 eV.[32] These $CH_3NH_3Pb(SCN)_2I$ films were found to be much more stable after 4 h in air with 95% humidity compared to MAPI films.[36] The reason for this stability, however, is not explained. Overall, the $CH_3NH_3Pb(SCN)_2I$ films displayed an efficiency of 8.3%, with a larger open circuit voltage (0.87 eV versus 0.80 eV), but a smaller fill factor (52 versus 63) than MAPI films.[32]

Very recently, Daub and Hillebrecht have reported that the reaction of MAI and $Pb(SCN)_2$ results in the formation of $(CH_3NH_3)_2Pb(SCN)_2I_2$ (herein denoted MAPSI).[33] MAPSI crystallizes in a layered orthorhombic pattern with space group $Pnm2_1$, in which the Pb is octahedrally coordinated to four axial I^- and two apical (or trans) S-bonded SCN^- ions. The MA

Received: September 30, 2015
Accepted: November 2, 2015
Published: November 2, 2015

DOI: 10.1021/acs.jpclett.5b02177
J. Phys. Chem. Lett. 2015, 6, 4594−4598

molecules are situated between the layers, resulting in a structure that is similar to the K_2NiF_4-type structure, as indicated in Figure 1. Daub and Hillebrecht demonstrated that the X-ray diffraction

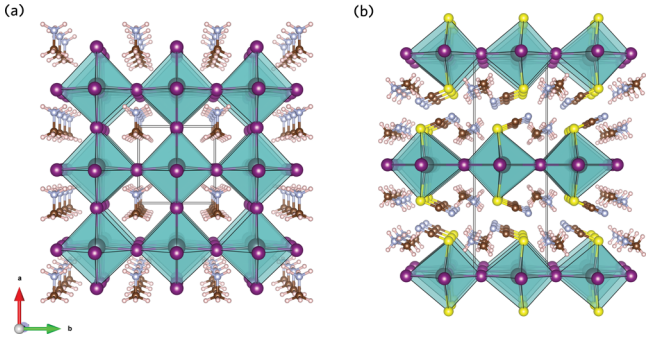

Figure 1. Crystal structure of (a) $CH_3NH_3PbI_3$ and (b) $(CH_3NH_3)_2Pb(SCN)_2I_2$ as viewed along the [001] direction. Pb, I, C, H, N, and S atoms are denoted by dark gray, purple, brown, pink, light gray/blue, and yellow spheres, respectively. The octahedral nature of the Pb is illustrated using turquoise polyhedra.

(XRD) pattern for MAPSI is actually an excellent fit for the XRD patterns of the $CH_3NH_3PbSCN_2I$ films produced by Jiang et al.[32]

Intriguingly for a 2D layered inorganic hybrid halide, MAPSI possesses an optical band gap of 1.56 eV, very close to that of quasi-cubic MAPI.[12,37] Typically, upon moving from a 3D to a 2D connectivity of the Pb-halide octahedra, the band gap opens up,[38,39] severely affecting solar cell absorber ability. Therefore, an open question remains: why can MAPSI possess a smaller band gap than other 2D hybrid halides?

In this Letter we investigate the fundamental electronic structure of MAPSI using hybrid density functional theory (DFT). We demonstrate: (i) that MAPSI does indeed possess a band gap suitable for PV applications, and explain why this is so via a detailed comparison with the electronic structure of MAPI, and (ii) show that MAPSI should be more stable against decomposition than MAPI. Lastly we speculate on the ability of this system to be the parent for other MAPSI structured hybrid halide-pseudohalide photovoltaic (PV) absorbers.

Computational Methods. All of our DFT calculations were performed using the Vienna Ab initio Simulation Package (VASP),[40−43] with interactions between the core and valence electrons described using the Projector Augmented Wave (PAW) method.[44] Electronic properties were calculated using the Heyd−Scuseria−Ernzerhof (HSE06) hybrid DFT functional[45] with the addition of spin orbit effects, which is known to accurately predict the properties of hybrid halide perovskite systems.[46] Both k-point sampling and the plane wave basis set were checked for convergence, with a cutoff of 520 eV and k-point grid of Γ-centered 1 × 4 × 4 for the 50 atom unit cell of $(CH_3NH_3)_2Pb(SCN)_2I_2$ found to be sufficient. The structure was geometrically optimized and considered to be converged when the forces on all the atoms totalled less than 10 meV $Å^{-1}$.

Geometry. We have minimized the experimental structure of MAPSI using three functionals, the Perdew, Burke, and Ernzerhof (PBE)[47] functional revised for solids (PBEsol),[48] PBEsol plus the addition of Grimme's D3 dispersion correction (PBEsol+D3),[49] and the PBE functional plus the addition of D3 (PBE+D3), with the results presented in Table 1. PBEsol and PBE+D3 yield structures in good agreement with the single crystal experimental structure,[33] whereas the PBEsol+D3 appears to underestimate the lattice constants more drastically.

Table 1. Calculated Lattice Parameters of $(CH_3NH_3)_2Pb(SCN)_2I_2$[a]

	a (Å)	*b* (Å)	*c* (Å)	volume (Å^3)
PBEsol	18.268 (−1.67%)	6.230 (−0.58%)	6.475 (+0.13%)	736.917 (−2.12%)
PBEsol+D3	17.657 (−4.97%)	6.134 (−2.12%)	6.388 (−1.21%)	691.872 (−8.10%)
PBE+D3	18.232 (−1.87%)	6.274 (+0.11%)	6.525 (+0.92%)	746.379 (−0.87%)
experiment[33]	18.580(2)	6.267(7)	6.466(6)	752.907

[a]Percentage difference from experiment or experimental error in brackets. All cell angles were found to be 90°. The equilibrium crystal structures are provided in an online repository.[50]

In all cases, the *a* parameter is underestimated compared to the experimental structure, indicating that thermal effects may play a role in determining the distance between the layers.

Electronic Structure. To test the effect of *a*-parameter variation on the electronic structure, we calculated the band structures at the experimental (room temperature, RT) coordinates and at the PBEsol structure, using the Heyd−Scuseria−Ernzerhof hybrid DFT functional[45] with the addition of spin orbit coupling (SOC) to accurately treat known relativistic effects experienced by lead-iodide-based hybrid halides. The lengthening of the *a* parameter shortens the calculated band gap of MAPSI from 1.79 to 1.57 eV (Figure S1 of the Supporting Information), remarkably close to the experimental optical band gap.[33] The partial (ion decomposed) density of states of MAPSI is presented in Figure 2a. It is immediately clear that the valence band maximum (VBM) is dominated by I *p* states with some Pb *s* states present, with the conduction band minimum (CBM) dominated by Pb *p* states, similar to to the electronic structure of MAPI (Figure 2c). The main difference stems from the N *p* and S *p* states, which are present ∼1 eV below the valence band maximum.

In semiconductors, *d*−*p* repulsion has been shown to play a role in determining the absolute ionization potential and, as such, the position of the VBM.[51] Comparison of the Pb *d* states in MAPSI against those in MAPI reveals an average shift in energy of only 0.15 eV, indicating a slight increase in Pb 5*d*−I 5*p* repulsion but unlikely to be sufficient to account for the smaller than expected band gap. Instead, the SCN states must act to push up the VBM of MAPSI, maintaining a small band gap despite the layered nature of the system. This is corroborated by analysis of the S−C−N bond lengths, which reveals an increase in the covalent character of the pseudohalide, as evidenced by the shortening of the S−C and lengthening of the C−N bonds in MAPSI (S−C = 1.601 eV, C−N = 1.169 eV) when compared to the ionic AgSCN (S−C = 1.783 eV, C−N = 1.144 eV).[52] The SCN therefore plays an active role in bonding, in contrast to other polyanion substituted MAPI structures,[53] which is supported by the charge density isosurfaces presented in Figure 3. Here, it can be seen that the VBM is dominated by Pb 6*p*/I 5*p* with a small contribution from the S 3*p* and N 2*p* of the SCN, with the CBM dominated by Pb 6*p* states.

The HSE06+SOC-calculated band gap for the RT MAPSI structure is presented in Figure 2b. The fundamental band gap is 1.57 eV, with the CBM and VBM situated just off the U point (0.0, 0.5, 0.5). There is noticeably no dispersion in the X−S direction, which is to be expected as this spans across the layers in the [100] direction. The calculations indicate that mild relativistic Dresselhaus splitting is present in the lower conduction band, and to a lesser extent in the upper valence band, due to the lack of the inversion symmetry in the MAPSI

DOI: 10.1021/acs.jpclett.5b02177
J. Phys. Chem. Lett. 2015, 6, 4594−4598

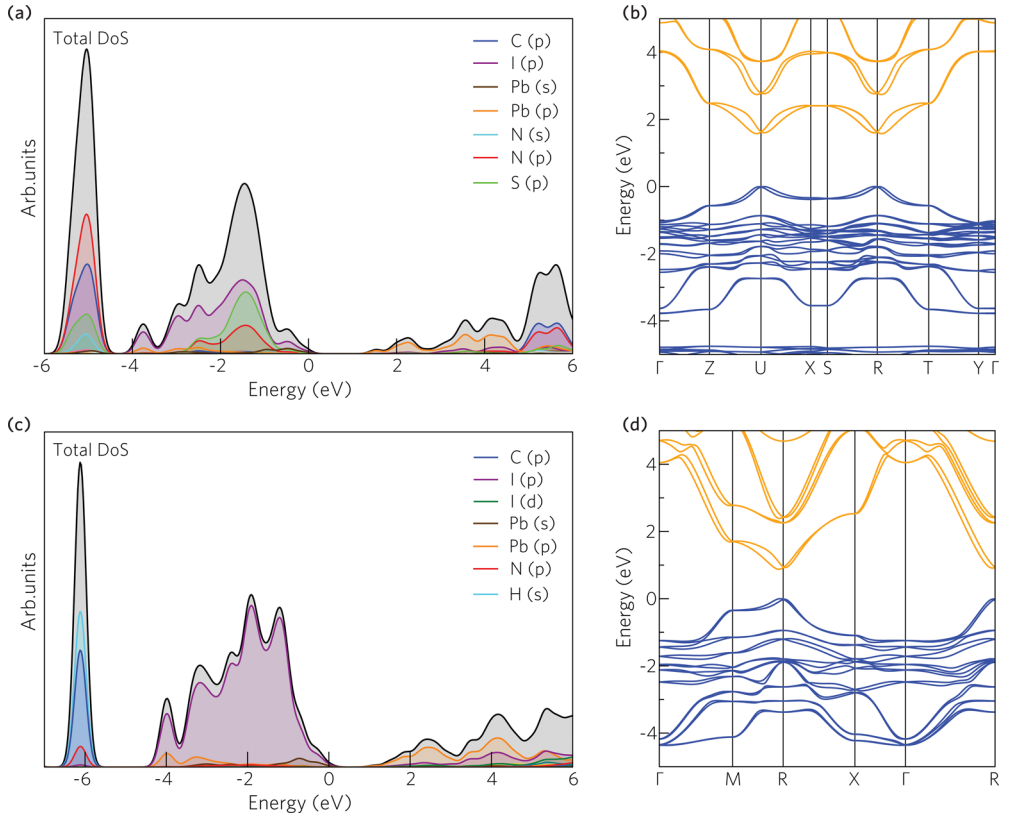

Figure 2. (a,c) Ion decomposed partial and total density of states and (b,d) band structure along the high symmetry directions for $(CH_3NH_3)_2Pb(SCN)_2I_2$ and $CH_3NH_3PbI_3$, respectively. In all cases, the HSE06+SOC method was used, and the VBM is set to 0 eV. The valence band and conduction band of panels b and d are denoted by blue and orange, respectively.

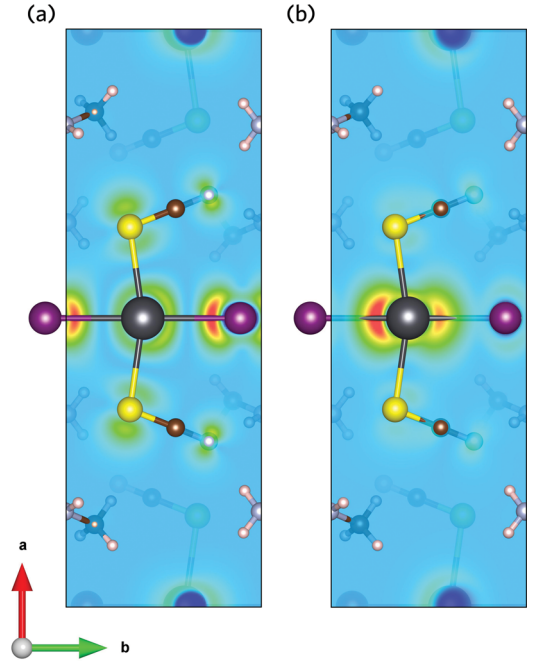

Figure 3. Charge density isosurfaces of (a) the VBM and (b) the CBM. Regions of low and high electron density are shown in blue and red, respectively. Pb, I, C, H, N, and S atoms are denoted by dark gray, purple, brown, pink, light gray/blue, and yellow spheres, respectively.

structure. We note that similar Dresselhaus splitting has previously been predicted for BF_4-substituted MAPI.[53]

The average effective masses of the VBM and CBM were found to be 0.20 m_0 and 0.14 m_0, respectively, indicating that both electrons and holes will be mobile in the MAPSI system, although the conductivity should be somewhat anisotropic due to its layered nature. We also tested the effect of SOC on the electronic structure of this system, with the results displayed in Figure S2 of the Supporting Information. Similar to MAPI,[54,55] the relativistic renormalization of the conduction band is large (~0.68 eV), indicating that proper treatment of relativistic effects is of vital importance. It should be noted that many body effects will also likely play a role in this Pb−I based system,[56,57] although the size of the MAPSI unit cell (50 atoms) means they are currently beyond the scope of this study.

Stability. The chemical stability of MAPI has been the subject of much debate in the past half decade.[20,21] It has been suggested that moisture or oxygen in the environment causes the poor stability of MAPI films,[24,36] but recent theoretical analysis suggests that the material is intrinsically thermodynamically unstable with respect to phase separation into PbI_2 and CH_3NH_3I.[58] To test the stability of MAPSI with regard to decomposition, we have tested two decomposition pathways, with their energetics compared to the decomposition of MAPI:

$$CH_3NH_3PbI_3 \rightarrow CH_3NH_3I + PbI_2, \quad \Delta_R H = -0.09 \text{ eV} \tag{1}$$

$$(CH_3NH_3)_2Pb(SCN)_2I_2 \rightarrow 2CH_3NH_3I + Pb(SCN)_2, \quad \Delta_R H = 0.38 \text{ eV} \tag{2}$$

DOI: 10.1021/acs.jpclett.5b02177
J. Phys. Chem. Lett. 2015, 6, 4594−4598

$$(CH_3NH_3)_2Pb(SCN)_2I_2 \rightarrow 2CH_3NH_3(SCN) + PbI_2, \quad \Delta_R H = 1.97\ \text{eV} \quad (3)$$

We find that the decomposition routes into either CH_3NH_3I and $Pb(SCN)_2$ (the starting materials in the synthesis of MAPSI) or $CH_3NH_3(SCN)$ and PbI_2 are both positive, indicating that MAPSI does not spontaneously decompose, unlike MAPI, in which it is favorable to decompose to CH_3NH_3I and PbI_2. This is the likely origin of the increased stability reported for materials with SCN incorporation.

We have demonstrated using DFT that MAPSI has an appropriate electronic structure for PV application, displaying a band gap of ∼1.57 eV, low effective masses for both holes and electrons, and improved chemical stability against phase separation when compared to MAPI. Experimentally, the addition of MAPSI to MAPI films seems to promote stability, and to be able to maintain reasonable efficiencies.[30] Interestingly, these results open up some fundamental questions. As ABX_3 perovskite structured MAPI can be electronically tuned by substitution on the A, B, and X sites, can MAPSI also act as a parent compound for a range of MAPSI structured analogues? Chemically, it should be possible to replace CH_3NH_3 with alternative organic molecules, Pb with Sn, I with Cl and Br, and even SCN with other pseudohalides such as SeCN and OCN. MAPSI, therefore, represents a novel material class with four degrees of freedom for property tuning. It is clear that further work on this new hybrid halide structural motif is warranted.

■ ASSOCIATED CONTENT

Supporting Information

The Supporting Information is available free of charge on the ACS Publications website at DOI: 10.1021/acs.jpclett.5b02177.

Effect of *a* parameter on the band gap of MAPSI; relativistic effects on the band structure of MAPSI (PDF)

■ AUTHOR INFORMATION

Corresponding Author

*E-mail: d.scanlon@ucl.ac.uk.

Notes

The authors declare no competing financial interest.

■ ACKNOWLEDGMENTS

We wish to thank Prof. Dr. Harald Hillebrecht for providing us with the experimental crystal structure of $(CH_3NH_3)_2Pb(SCN)_2I_2$. This work made use of the ARCHER U.K. National Supercomputing Service (http://www.archer.ac.uk), via our membership of the U.K.'s HEC Materials Chemistry Consortium, which is funded by EPSRC (EP/L000202), the Iridis cluster, provided by the EPSRC funded Centre for Innovation (Grant codes EP/K000144/1 and EP/K000136/1) and the UCL Legion HPC Facility (Legion@UCL). A.M.G. acknowledges Diamond Light Source and the M3S CDT at UCL for the cosponsorship of a studentship. C.N.S. is grateful to EPSRC and the Department of Chemistry at UCL for the provision of a DTA studentship.

■ REFERENCES

(1) Grätzel, M. The light and shade of perovskite solar cells. *Nat. Mater.* **2014**, *13*, 838−842.

(2) Green, M. A.; Ho-Baillie, A.; Snaith, H. J. The emergence of perovskite solar cells. *Nat. Photonics* **2014**, *8*, 506−514.

(3) Park, N.-G. Organometal Perovskite Light Absorbers Toward a 20% Efficiency Low-Cost Solid-State Mesoscopic Solar Cell. *J. Phys. Chem. Lett.* **2013**, *4*, 2423−2429.

(4) Yang, W. S.; Noh, J. H.; Jeon, N. J.; Kim, Y. C.; Ryu, S.; Seo, J.; Seok, S. I. High-performance photovoltaic perovskite layers fabricated through intramolecular exchange. *Science* **2015**, *348*, 1234−1237.

(5) Komiya, R.; Fukui, A.; Murofushi, N.; Koide, N.; Yamanaka, R.; Katayama, H. Improvement of the conversion efficiency of a monolithic type dyesensitized solar cell module. *Technical Digest of the 21st International Photovoltaic Science and Engineering Conference*, 2C-5O-08, Fukuoka, Japan. 2011.

(6) Hosoya, M.; Oooka, H.; Nakao, H.; Gotanda, T.; Mori, S.; Shida, N.; Hayase, R.; Nakano, Y.; Saito, M. Organic thin film photovoltaic modules. *Proceedings, 93rd Annual Meeting of The Chemical Society of Japan*, 2013; pp 21−37.

(7) Wang, W.; Winkler, M. T.; Gunawan, O.; Gokmen, T.; Todorov, T. K.; Zhu, Y.; Mitzi, D. B. Device Characteristics of CZTSSe Thin-Film Solar Cells with 12.6% Efficiency. . *Adv. Energy Mater.* **2014**, *4*, 1301465.

(8) Kim, H.-S.; Im, S. H.; Park, N.-G. Organolead Halide Perovskite: New Horizons in Solar Cell Research. *J. Phys. Chem. C* **2014**, *118*, 5615−5625.

(9) Hodes, G.; Cahen, D. Photovoltaics: Perovskite cells roll forward. *Nat. Photonics* **2014**, *8*, 87−88.

(10) Bhachu, D. S.; Scanlon, D. O.; Saban, E. J.; Bronstein, H.; Parkin, I. P.; Carmalt, C. J.; Palgrave, R. G. Scalable route to $CH_3NH_3PbI_3$ perovskite thin films by aerosol assisted chemical vapour deposition. *J. Mater. Chem. A* **2015**, *3*, 9071−9073.

(11) Barrows, A. T.; Pearson, A. J.; Kwak, C. K.; Dunbar, A. D. F.; Buckley, A. R.; Lidzey, D. G. Efficient planar heterojunction mixed-halide perovskite solar cells deposited via spray-deposition. *Energy Environ. Sci.* **2014**, *7*, 2944.

(12) Baikie, T.; Fang, Y.; Kadro, J. M.; Schreyer, M.; Wei, F.; Mhaisalkar, S. G.; Graetzel, M.; White, T. J. Synthesis and crystal chemistry of the hybrid perovskite $(CH_3NH_3)PbI_3$ for solid-state sensitised solar cell applications. *J. Mater. Chem. A* **2013**, *1*, 5628−5641.

(13) D'Innocenzo, V.; Grancini, G.; Alcocer, M. J.; Kandada, A. R. S.; Stranks, S. D.; Lee, M. M.; Lanzani, G.; Snaith, H. J.; Petrozza, A. Excitons versus free charges in organo-lead tri-halide perovskites. *Nat. Commun.* **2014**, *5*, 3586.

(14) Deng, Y.; Peng, E.; Shao, Y.; Xiao, Z.; Dong, Q.; Huang, J. Scalable fabrication of efficient organolead trihalide perovskite solar cells with doctor-bladed active layers. *Energy Environ. Sci.* **2015**, *8*, 1544−1550.

(15) Xing, G.; Mathews, N.; Sun, S.; Lim, S. S.; Lam, Y. M.; Gratzel, M.; Mhaisalkar, S.; Sum, T. C. Long-Range Balanced Electron- and Hole-Transport Lengths in Organic-Inorganic $CH_3NH_3PbI_3$. *Science* **2013**, *342*, 344−347.

(16) Walsh, A.; Scanlon, D. O.; Chen, S.; Gong, X. G.; Wei, S.-H. Self-Regulation Mechanism for Charged Point Defects in Hybrid Halide Perovskites. *Angew. Chem.* **2015**, *127*, 1811−1814.

(17) Shao, Y.; Xiao, Z.; Bi, C.; Yuan, Y.; Huang, J. Origin and elimination of photocurrent hysteresis by fullerene passivation in $CH_3NH_3PbI_3$ planar heterojunction solar cells. *Nat. Commun.* **2014**, *5*, 5784.

(18) Wehrenfennig, C.; Eperon, G. E.; Johnston, M. B.; Snaith, H. J.; Herz, L. M. High Charge Carrier Mobilities and Lifetimes in Organolead Trihalide Perovskites. *Adv. Mater.* **2014**, *26*, 1584−1589.

(19) Zhao, Y.; Zhu, K. Charge Transport and Recombination in Perovskite $(CH_3NH_3)PbI_3$ Sensitized TiO_2 Solar Cells. *J. Phys. Chem. Lett.* **2013**, *4*, 2880−2884.

(20) Guarnera, S.; Abate, A.; Zhang, W.; Foster, J. M.; Richardson, G.; Petrozza, A.; Snaith, H. J. Improving the Long-Term Stability of Perovskite Solar Cells with a Porous Al_2O_3 Buffer Layer. *J. Phys. Chem. Lett.* **2015**, *6*, 432−437.

(21) Niu, G.; Guo, X.; Wang, L. Review of Recent Progress in Chemical Stability of Perovskite Solar Cells. *J. Mater. Chem. A* **2015**, *3*, 8970−8980.

(22) Han, Y.; Meyer, S.; Dkhissi, Y.; Weber, K.; Pringle, J.; Bach, U.; Spiccia, L.; Cheng, Y.-B. Degradation observations of encapsulated

DOI: 10.1021/acs.jpclett.5b02177
J. Phys. Chem. Lett. 2015, 6, 4594−4598

planar $CH_3NH_3PbI_3$ perovskite solar cells at high temperatures and humidity. *J. Mater. Chem. A* **2015**, *3*, 8139−8147.
(23) Kempe, M. D.; Dameron, A. A.; Reese, M. O. Evaluation of moisture ingress from the perimeter of photovoltaic modules. *Prog. Photovoltaics* **2014**, *22*, 1159−1171.
(24) Burschka, J.; Pellet, N.; Moon, S.-J.; Humphry-Baker, R.; Gao, P.; Nazeeruddin, M. K.; Grätzel, M. Sequential deposition as a route to high-performance perovskite-sensitized solar cells. *Nature* **2013**, *499*, 316−319.
(25) Pisoni, A.; Jaćimović, J.; Barišić, O. S.; Spina, M.; Gaál, R.; Forró, L.; Horváth, E. Ultra-Low Thermal Conductivity in Organic-Inorganic Hybrid Perovskite $CH_3NH_3PbI_3$. *J. Phys. Chem. Lett.* **2014**, *5*, 2488−2492.
(26) Li, X.; Tschumi, M.; Han, H.; Babkair, S. S.; Alzubaydi, R. A.; Ansari, A. A.; Habib, S. S.; Nazeeruddin, M. K.; Zakeeruddin, S. M.; Grätzel, M. Outdoor Performance and Stability under Elevated Temperatures and Long-Term Light Soaking of Triple-Layer Mesoporous Perovskite Photovoltaics. *Energy Technology* **2015**, *3*, 551−555.
(27) Habisreutinger, S. N.; Leijtens, T.; Eperon, G. E.; Stranks, S. D.; Nicholas, R. J.; Snaith, H. J. Enhanced Hole Extraction in Perovskite Solar Cells Through Carbon Nanotubes. *J. Phys. Chem. Lett.* **2014**, *5*, 4207−4212.
(28) Liu, J.; Wu, Y.; Qin, C.; Yang, X.; Yasuda, T.; Islam, A.; Zhang, K.; Peng, W.; Chen, W.; Han, L. A dopant-free hole-transporting material for efficient and stable perovskite solar cells. *Energy Environ. Sci.* **2014**, *7*, 2963.
(29) Leo, K. Perovskite photovoltaics: Signs of stability. *Nat. Nanotechnol.* **2015**, *10*, 574−575.
(30) Chen, Y.; Li, B.; Huang, W.; Gao, D.; Liang, Z. Efficient and reproducible $CH_3NH_3PbI_{3-x}(SCN)_x$ perovskite based planar solar cells. *Chem. Commun.* **2015**, *51*, 11997−11999.
(31) Halder, A.; Chulliyil, R.; Subbiah, A. S.; Khan, T.; Chattoraj, S.; Chowdhury, A.; Sarkar, S. K. Pseudo-halide (SCN^-) doped $MAPbI_3$ Perovskites: A Few Surprises. *J. Phys. Chem. Lett.* **2015**, *6*, 3483−3489.
(32) Jiang, Q.; Rebollar, D.; Gong, J.; Piacentino, E. L.; Zheng, C.; Xu, T. Pseudohalide-Induced Moisture Tolerance in Perovskite $CH_3NH_3Pb(SCN)_2I$ Thin Films. *Angew. Chem., Int. Ed.* **2015**, *54*, 7617−7620.
(33) Daub, M.; Hillebrecht, H. Synthesis, Single-Crystal Structure and Characterization of $(CH_3NH_3)_2Pb(SCN)_2I_2$. *Angew. Chem.* **2015**, *127*, 11168−11169.
(34) Kim, H.-S.; Park, N.-G. Parameters Affecting I-V Hysteresis of $CH_3NH_3PbI_3$ Perovskite Solar Cells: Effects of Perovskite Crystal Size and Mesoporous TiO_2 Layer. *J. Phys. Chem. Lett.* **2014**, *5*, 2927−2934.
(35) Snaith, H. J.; Abate, A.; Ball, J. M.; Eperon, G. E.; Leijtens, T.; Noel, N. K.; Stranks, S. D.; Wang, J. T.-W.; Wojciechowski, K.; Zhang, W. Anomalous Hysteresis in Perovskite Solar Cells. *J. Phys. Chem. Lett.* **2014**, *5*, 1511−1515.
(36) Niu, G.; Li, W.; Meng, F.; Wang, L.; Dong, H.; Qiu, Y. Study on the stability of $CH_3NH_3PbI_3$ films and the effect of post-modification by aluminum oxide in all-solid-state hybrid solar cells. *J. Mater. Chem. A* **2014**, *2*, 705−710.
(37) Noh, J. H.; Im, S. H.; Heo, J. H.; Mandal, T. N.; Seok, S. I. Chemical Management for Colorful, Efficient, and Stable Inorganic-Organic Hybrid Nanostructured Solar Cells. *Nano Lett.* **2013**, *13*, 1764−1769.
(38) Smith, I. C.; Hoke, E. T.; Solis-Ibarra, D.; McGehee, M. D.; Karunadasa, H. I. A Layered Hybrid Perovskite Solar-Cell Absorber with Enhanced Moisture Stability. *Angew. Chem., Int. Ed.* **2014**, *53*, 11232−11235.
(39) Stoumpos, C. C.; Malliakas, C. D.; Kanatzidis, M. G. Semiconducting Tin and Lead Iodide Perovskites with Organic Cations: Phase Transitions, High Mobilities, and Near-Infrared Photoluminescent Properties. *Inorg. Chem.* **2013**, *52*, 9019−9038.
(40) Kresse, G.; Hafner, J. *Ab initio* molecular dynamics for liquid metals. *Phys. Rev. B: Condens. Matter Mater. Phys.* **1993**, *47*, 558−561.
(41) Kresse, G.; Hafner, J. *Ab initio* molecular-dynamics simulation of the liquid-metal amorphous-semiconductor transition in germanium. *Phys. Rev. B: Condens. Matter Mater. Phys.* **1994**, *49*, 14251−14269.
(42) Kresse, G.; Furthmüller, J. Efficient iterative schemes for ab initio total-energy calculations using a plane-wave basis set. *Phys. Rev. B: Condens. Matter Mater. Phys.* **1996**, *54*, 11169−11186.
(43) Kresse, G.; Furthmüller, J. Efficiency of ab initio total energy calculations for metals and semiconductors using a plane wave basis set. *Comput. Mater. Sci.* **1996**, *6*, 15.
(44) Kresse, G.; Joubert, D. From ultrasoft pseudopotentials to the projector augmented-wave method. *Phys. Rev. B: Condens. Matter Mater. Phys.* **1999**, *59*, 1758−1775.
(45) Krukau, A. V.; Vydrov, O. A.; Izmaylov, A. F.; Scuseria, G. E. Influence of the exchange screening parameter on the performance of screened hybrid functionals. *J. Chem. Phys.* **2006**, *125*, 224106.
(46) Yin, W.-J.; Yang, J.-H.; Kang, J.; Yan, Y.; Wei, S.-H. Halide perovskite materials for solar cells: a theoretical review. *J. Mater. Chem. A* **2015**, *3*, 8926−8942.
(47) Perdew, J. P.; Burke, K.; Ernzerhof, M. Generalized Gradient Approximation Made Simple. *Phys. Rev. Lett.* **1996**, *77*, 3865−3868.
(48) Perdew, J. P.; Ruzsinszky, A.; Csonka, G. I.; Vydrov, O. A.; Scuseria, G. E.; Constantin, L. A.; Zhou, X.; Burke, K. Restoring the Density-Gradient Expansion for Exchange in Solids and Surfaces. *Phys. Rev. Lett.* **2008**, *100*, 136406.
(49) Grimme, S. Accurate description of van der Waals complexes by density functional theory including empirical corrections. *J. Comput. Chem.* **2004**, *25*, 1463−1473.
(50) https://github.com/SMTG-UCL/MAPSI, Accessed: 2015-10-04.
(51) Wei, S.-H.; Zunger, A. Role of metal d states in II-VI semiconductors. *Phys. Rev. B: Condens. Matter Mater. Phys.* **1988**, *37*, 8958.
(52) Williams, D. J.; Daemen, L.; Vogel, S.; Proffen, T. Temperature dependence of the crystal structure of α-AgSCN by powder neutron diffraction. *J. Appl. Crystallogr.* **2007**, *40*, 1039−1043.
(53) Hendon, C. H.; Yang, R. X.; Burton, L. A.; Walsh, A. Assessment of polyanion (BF_4^- and PF_6^-) substitutions in hybrid halide perovskites. *J. Mater. Chem. A* **2015**, *3*, 9067−9070.
(54) Even, J.; Pedesseau, L.; Jancu, J.-M.; Katan, C. Importance of Spin−Orbit Coupling in Hybrid Organic/Inorganic Perovskites for Photovoltaic Applications. *J. Phys. Chem. Lett.* **2013**, *4*, 2999−3005.
(55) Frost, J. M.; Butler, K. T.; Brivio, F.; Hendon, C. H.; van Schilfgaarde, M.; Walsh, A. Atomistic Origins of High-Performance in Hybrid Halide Perovskite Solar Cells. *Nano Lett.* **2014**, *14*, 2584−2590.
(56) Mosconi, E.; Amat, A.; Nazeeruddin, M. K.; Grätzel, M.; De Angelis, F. First-Principles Modeling of Mixed Halide Organometal Perovskites for Photovoltaic Applications. *J. Phys. Chem. C* **2013**, *117*, 13902−13913.
(57) Butler, K. T.; Frost, J. M.; Walsh, A. Band alignment of the hybrid halide perovskites $CH_3NH_3PbCl_3$, $CH_3NH_3PbBr_3$ and $CH_3NH_3PbI_3$. *Mater. Horiz.* **2015**, *2*, 228−231.
(58) Zhang, Y.-Y.; Chen, S.; Xu, P.; Xiang, H.; Gong, X.-G.; Walsh, A.; Wei, S.-H. Intrinsic Instability of the Hybrid Halide Perovskite Semiconductor $CH_3NH_3PbI_3$. *arXiv:1506.01301 [cond-mat.mtrl-sci]*, 2015.

■ NOTE ADDED AFTER ASAP PUBLICATION

This paper was published ASAP on November 6, 2015. Equations 1−3 were updated. The revised paper was reposted on November 11, 2015.

DOI: 10.1021/acs.jpclett.5b02177
J. Phys. Chem. Lett. 2015, 6, 4594−4598